

Large-scale and local-scale structures in polymer-blend films: a grazing-incidence ultra-small-angle X-ray scattering and sub-microbeam grazing-incidence small-angle X-ray scattering investigation

P. Müller-Buschbaum,^{a*} E. Bauer,^a E. Maurer,^a S. V. Roth,^b R. Gehrke,^b M. Burghammer^c and C. Riekell^c

^aTU München, Physik-Department, LS E13, James-Frank-Str.1, 85747 Garching, Germany, ^bHASYLAB at DESY, Notkestr. 85, 22603 Hamburg, Germany, and ^cESRF, BP 220, F-38043 Grenoble Cedex 09, France.
Correspondence e-mail: muellerb@ph.tum.de

Phase-separation structures are installed by solution casting and flow of a binary polymer-blend solution of polystyrene and poly-*n*-butylacrylate in toluene on silicon. Optical microscopy and scanning-probe microscopy measurements provide the surface topography. Large-scale structures are probed with high-resolution or grazing-incidence ultra-small-angle X-ray scattering enabled by high reciprocal-space resolution. Correspondingly, structures of up to 13 μm are resolved. Local-scale structures are detected with sub-microbeam grazing-incidence small-angle X-ray scattering, providing a high real-space resolution of 1 μm . Nanometre-size cavities are found in the polystyrene-rich parts of the blend film.

© 2007 International Union of Crystallography
Printed in Great Britain – all rights reserved

1. Introduction

Blending different polymers and thereby obtaining new and tailored material properties is one of the bases of the success of polymer applications (Hashimoto, 1993). One prominent example is the tailoring of mechanical properties by mixing soft and hard polymer components, or combining a polymer with a glass transition temperature well above room temperature with one well below. Coating solid surfaces with such polymer blends and conserving the properties of the bulk blend material in the blend film is an extremely attractive way to obtain functional coatings (Ryan, 2002). Large-scale phase-separation structures are typically formed due to the immiscibility of the blended polymers (Tanaka, 2000), ensuring a variety of applications, *e.g.* in optics or sensors (Walheim *et al.*, 1999). The morphology is altered and tailored by changing the ratio of the components in the blend (Gutmann *et al.*, 1999). The characteristic structural size is modified through the amount of material deposited on the solid support and by the preparation technique used. As recently demonstrated, the use of flow allows the creation of superstructures and thus enlarges the range of accessible structures compared to simple phase separation (Müller-Buschbaum *et al.*, 2006).

The resulting surface structures are easily probed in real space with optical and scanning-probe techniques. The large-scale structures and the flow-induced superstructures are pictured optically. Scanning-probe techniques provide topography information with mechanical contrast. However, non-destructive access to the interior of the blend films is impossible with both experimental methods.

Over the past few years, grazing-incidence small-angle X-ray scattering (GISAXS), pioneered by Levine *et al.* (1989), has turned out to be a powerful experimental tool which provides this information. The X-ray beam falls onto the sample surface at a very small incident angle and the scattering intensity is collected with a two-

dimensional (2D) detector placed at the desired distance behind the sample. Contrary to the typical slab-like beams in reflectivity experiments, a point-like beam is required. Following the ideas of standard transmission small-angle X-ray scattering experiments, the reciprocal space of interest is selected by the sample-to-detector distance used and the resolution is chosen accordingly (Gibaud *et al.*, 2003). The two-dimensional intensity distribution can be understood as an assembly of several vertical and horizontal slices (Salditt *et al.*, 1995). With the sample surface defining the (*x*, *y*) plane and the incidence beam being directed along the *x* axis, the GISAXS signal is analyzed along the *y* direction. Historically, such horizontal (with respect to the sample surface) cuts of 2D intensity distributions, obtained from the two-dimensional detector array, were called out-of-plane scans.

Besides material classes with a high X-ray scattering contrast, such as self-organized inorganic monodisperse nano-objects (Renaud *et al.*, 2003), polymer films are also routinely probed (Müller-Buschbaum, 2003a). Films of laterally homogeneous composition are typically investigated. Examples of nanometre-size structures in polymer films are microphase-separation structures in block copolymer films (Papadakis *et al.*, 2004) and polymeric nanodots (Müller-Buschbaum *et al.*, 1997).

In this article we describe recent experimental improvements which overcome both restrictions of GISAXS: the need for sample homogeneity and the quite small upper limit of the detectable structural size. Both of the experimental developments of GISAXS presented here rely on focusing the X-ray beam. The focusing of the beam onto the sample position results in high real-space resolution at the position of the sample (Riekell, 2000). As a consequence, micro-focused beams combined with GISAXS and scanning of the sample with respect to the beam allow local structures to be probed instead of homogeneous samples (Müller-Buschbaum *et al.*, 2003). In contrast, focusing the X-ray beam on the detector yields high reci-

procal-space resolution, which is necessary for probing large-scale structures.

The possibilities offered by such advanced GISAXS setups are demonstrated in this article with the model system of a binary polymer-blend film. Large-scale structures are an intrinsic feature of such blend films. The sample heterogeneity is introduced by the superposition of phase separation and flow (Yang & Han, 1996).

2. Experimental

2.1. Sample preparation

To ensure a well controlled surface chemistry, native-oxide-covered Si(100) surfaces (CrysTec Kristalltechnologie, Berlin) were cleaned prior to solution deposition (Müller-Buschbaum, 2003b). The acid cleaning process includes 15 min at 353 K in an acid bath consisting of 100 ml of 80% H₂SO₄, 35 ml H₂O₂ and 15 ml deionized water, rinsing in deionized water and drying with compressed oil-free nitrogen immediately before deposition of the blend solution. The model system used consists of blend films of polystyrene (PS) and poly-*n*-butylacrylate (PnBA) with molecular weights $M_w = 207 \text{ kg mol}^{-1}$ (molecular weight distribution $M_w/M_n = 1.02$) and $M_w = 260 \text{ kg mol}^{-1}$ ($M_w/M_n = 3.78$), respectively. With a ratio of 3:7 and 1:1 wt%, PS and PnBA were dissolved in toluene with concentrations of 0.98 to 5.0 mg ml⁻¹. Varying the solution concentration as well as the amount of solution deposited on the solid support enabled the installation of different polymer-film thicknesses. The smooth drying process in a specially designed sample chamber at ambient conditions resulted in dry polymer-blend films. Owing to the immiscibility of PS and PnBA [the polymer–polymer interaction parameter of PS and PnBA is 0.162 at 293 K (Stenert *et al.*, 2004)], these blend films show remarkable surface structures.

Two different orientations of the substrate were chosen: (a) The Si surface was carefully aligned perpendicular to the gravitational field. The full surface was covered with solution to obtain homogeneous films after drying (denoted solution casting). (b) The Si surface was slightly inclined ($\gamma = 0.6^\circ$) to the previous position, thereby enabling flow of the liquid. Instead of a full surface coverage, only a liquid ridge was deposited. The ridge slid down the incline while it was subjected to drying. Behind the ridge, a thin film of polymeric blend was deposited that turned out to have roughly periodically varying properties along the flow direction (Müller-Buschbaum *et al.*, 2006).

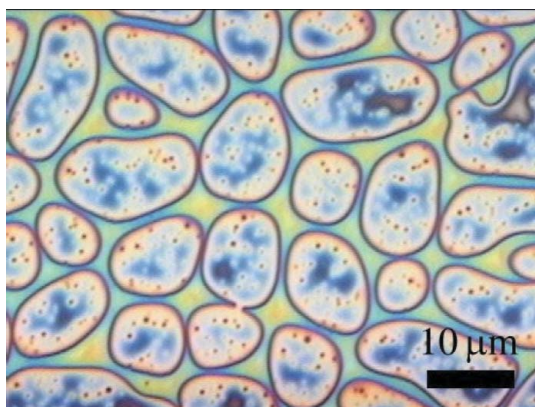


Figure 1
Optical micrograph picturing the marked phase-separation structure installed after solution casting of the PS:PnBA = 1:1–toluene solution with concentration of 5 mg ml⁻¹ on Si.

2.2. Real-space investigation

The sample surfaces were observed with optical microscopy using a Zeiss Axiotech 25H optical microscope with a magnification between 4 and 100 \times . A Hitachi KP-D50 CCD camera recorded the micrographs.

For improved lateral resolution, and also to obtain height and mechanical contrast information, scanning-probe microscopy (SPM) was used. An Autoprobe CP (Veeco) atomic force microscope was operated in tapping-mode conditions with gold-coated silicon cantilevers (Ultralever cantilevers). All measurements were performed under air and at room temperature. For each sample, micrographs at several different spatial positions of the surface were recorded. Scan ranges up to 60 $\mu\text{m} \times 60 \mu\text{m}$ were selected. The background due to the scanner-tube movement was fully subtracted from the raw data.

2.3. Grazing-incidence ultra-small-angle X-ray scattering

The high-resolution grazing-incidence small-angle X-ray scattering and grazing-incidence ultra-small-angle X-ray scattering (GIUSAXS) experiments were performed at the BW4 beamline (HASYLAB, Hamburg) using a wavelength of $\lambda = 0.138 \text{ nm}$. The X-ray beam pathway was evacuated to reduce background. The non-specular and specular intensities were recorded with a two-dimensional detector (MARCCD), which consists of a 2048 \times 2048 pixel array, as a function of the exit angle α_f and the out-of-plane angle Ψ . At the selected incident angle of $\alpha_i = 0.41^\circ$ both features (the specular peak and Yoneda peak) were well separated on the detector area along the vertical direction. This allowed a small beamstop to be used which only shadowed the specular peak (a second beamstop was used to block the direct beam) without shadowing the central part of the Yoneda peak as well. The beam divergence in and out of the reflection plane was set by two narrow entrance cross-slits together with focusing the X-ray beam on the detector to match the detector resolution in terms of pixel size (79 μm). A very large sample-to-detector distance of 13.0 m was chosen so that a resolution of approximately $2.75 \times 10^{-4} \text{ nm}^{-1}$ was achieved. The maximum accessible lateral length scale (21 μm) of this ultra high resolution setup was confirmed by means of Monte-Carlo ray tracing simulation of the beamline BW4.

2.4. Sub-microbeam grazing-incidence small-angle X-ray scattering

The sub-microbeam grazing incidence small-angle X-ray scattering (sub-microbeam GISAXS) experiments were performed at the ID13 beamline (ESRF, Grenoble). A wavelength of $\lambda = 0.097 \text{ nm}$ was chosen. Again, the non-specular and the specular intensity were recorded with a two-dimensional detector (MARCCD), which consisted of a 2048 \times 2048 pixel array. Instead of focusing on the detector, two crossed linear Fresnel-zone plates focused on the sample position. A beam with a diameter of 0.9 μm was used. Using a beam with this small diameter affects the upper limit of the detectable structure size. Structures of the size of the beam are not resolved and, moreover, the divergence of the focused beam reduces the largest detectable structure even further (Riekell, 2000). As a consequence, sub-micrometre-size X-ray beams are not suited to the study of large structures. Thus the sample-to-detector distance was set to a small value of 0.8 m, to emphasize small-scale structures instead. The shallow incident angle resulted in a footprint of the beam on the sample surface which is smeared along the beam direction. To obtain a reasonably long footprint of $0.9 \times 52.4 \mu\text{m}$, a fixed incident angle $\alpha_i = 0.983^\circ$ was selected. At smaller incident angles a larger footprint would have been the result. Consequently, the micro-focused beam

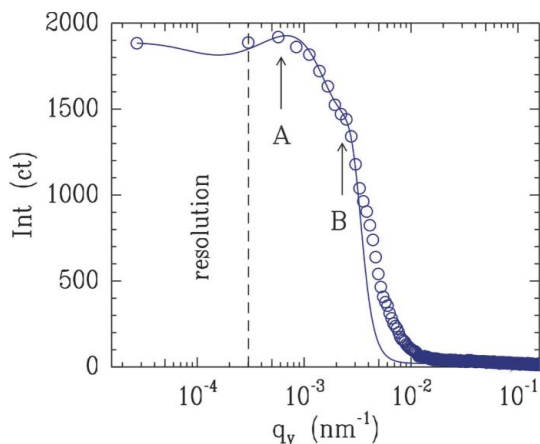


Figure 2
High-resolution GIUSAXS data (circles) displayed with a simple model (solid line) introducing two characteristic lateral lengths, denoted A and B.

transformed in the GISAXS geometry into a line shape and thereby allowed lateral structures to be probed by scanning the sample with respect to the X-ray beam position. A fixed beamstop was again used to shield the specular peak and therefore protect the detector.

3. Large-scale structures

Spin-coating of PS:PnBA–toluene solutions results in thin blend films with mesoscopic phase-separation structures (Stenert *et al.*, 2004). In addition, in the thin-film regime the interplay with dewetting has to be taken into account (Wang & Composto, 2003). Solution-casted films have larger thicknesses than spin-coated films. According to scaling laws, the increase in film thickness results in a coarsening of the structures installed by phase separation. Fig. 1 shows a typical optical micrograph picturing the structures in the case of a blend ratio 1:1. Large glassy PS domains are embedded in a matrix of PnBA. Using Fourier transformation, analysis of optical micrographs at several different sample positions and with different magnifications leads to a typical lateral length of 13 μm , which describes the structures at the film surface.

With typical GISAXS experiments, the detection of structures of this size is impossible. However, with GIUSAXS this large-scale structure is resolved. Fig. 2 shows a horizontal cut from the 2D intensity measured at BW4 using the setup described above. The cut was selected at the critical angle of PnBA. The lateral component – parallel to the sample surface and perpendicular to the X-ray beam direction – of the scattering vector is denoted by $q_y = 2\pi/\lambda(\sin \Psi \cos \alpha_i)$. The solid line is a fit assuming a model based on two structure-factor contributions and highly polydisperse form-factor contributions (see the real-space structure in Fig. 1). In addition,

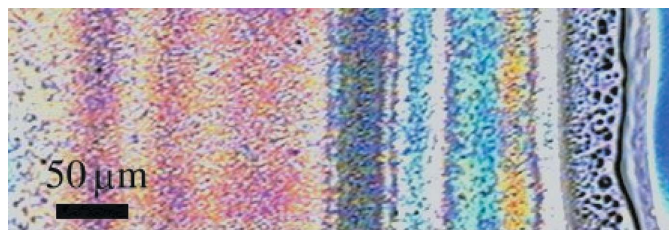


Figure 3
Optical micrograph showing the typical pattern installed by flow of a PS:PnBA = 3:7–toluene solution on an inclined Si surface with a concentration of 1 mg ml^{-1} .

tion, the resolution of the experimental setup is taken into account (Müller-Buschbaum, 2006).

Well outside the theoretical resolution limit obtained from ray tracing, two intensity features are visible. The peak in the intensity, labelled A, corresponds to the lateral length of 13 μm as probed with optical microscopy. Thus it resembles a surface feature of the blend film. Moreover, a shoulder in the intensity, labelled B, is visible as well. The corresponding lateral length is 2.2 μm and cannot be assigned to a surface feature. Therefore, with GIUSAXS an additional internal structure located within the blend film is detected which was not accessible with optics. At larger q_y values the data and the model deviate. This could originate from the presence of smaller structures which are not taken into account in the model. Alternatively, the polydispersity of the object shape might be overestimated. However, the good agreement at small q_y values demonstrates the ability to resolve several micrometre-size structures in the GISAXS geometry.

4. Local-scale structures

The interaction of evaporation and flow of a polymer blend solution on an inclined substrate produces complex multi-scale patterns (Müller-Buschbaum *et al.*, 2006). This patterning on the 100 μm scale induces a periodic variation in the locally homogeneous 1 μm -scale

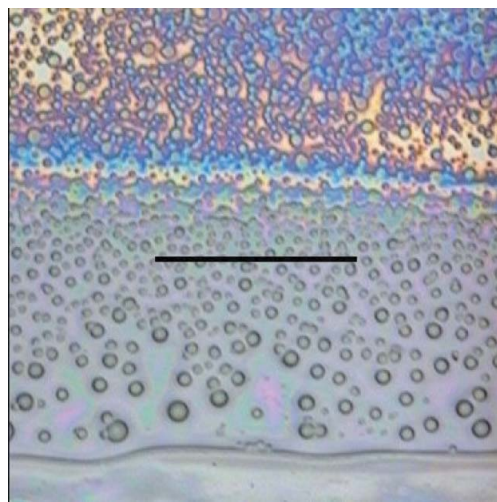


Figure 4
Optical micrograph picturing the region close to the bulge in a flow-induced structure (PS:PnBA = 3:7, 1 mg ml^{-1}). The solid line indicates the typical length of the X-ray footprint on the surface (52.4 μm). The flow is directed along the vertical axis.

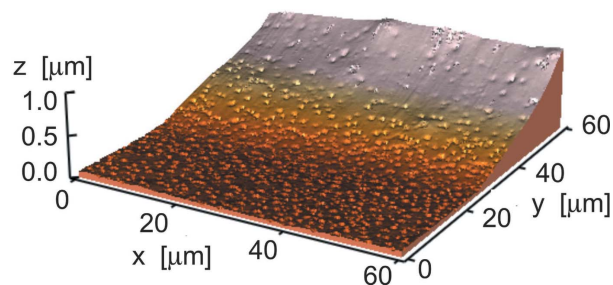


Figure 5
Three-dimensional view of the surface topography installed by flow along the y axis, sketching the drastic changes in height due to the creation of a polymeric bulge.

morphologies that result from phase separation in the deposited blend film. Fig. 3 shows a corresponding optical micrograph. The original flow direction was from top to bottom. The color changes indicate changes in the thickness and blend composition. In the bottom part of Fig. 4 a polymeric bulge is located. This bulge interrupts the region with alternating behavior. It has a mean thickness of several micrometres. The alternations have a characteristic length scale in the flow direction of about 50 μm . Perpendicular to the flow the morphology is homogeneous.

With SPM the topography is measured. For SPM data with small scan ranges the background due to the scanner movement is difficult to decouple from the height variation because of the polymer bulge. At large scan ranges a decoupling is possible. Thus the SPM data are flattened without removing the original height increase that was caused by the bulge. Fig. 5 shows a three-dimensional view of the scanned region close to the bulge. The scan does not cover the full bulge because the SPM scanner is limited in its z extension and tapping parameters are not easy to adjust to probe shallow film structures together with a strongly increasing height.

In order to focus on the lateral structures, which are difficult to see in the three-dimensional presentation as chosen in Fig. 5, the height increase due to the polymer bulge was removed from the SPM data. The resulting height data represent a skin-like topography. Fig. 6(a) shows these data with the typical height presentation, with deep structures shown as dark and high structures shown as light. From Fig. 6(a) it is obvious that the number of holes in the film surface increases from bottom to top. Hence the film is not homogeneous on the scale of 60 μm .

In addition to topography, SPM provides a mechanical contrast between the soft PnBA (glass transition temperature 230 K) and the rigid PS (glass transition temperature 377 K) regions. Fig. 6(b) shows the phase image. Soft regions are displayed as dark and rigid regions as light. From the bottom to the top the number of dark regions increases. Translated into composition information, this means that the blend ratio of 3:7 chosen originally is locally altered. In the bottom part PS is strongly enriched. Strictly speaking, only near-surface parts are probed because SPM does not access the material deep inside the film. However, it matches very nicely with previous observations obtained with scattering that the bulges are enriched with PS (Müller-Buschbaum *et al.*, 2006).

Moreover, the alteration of the blend ratio originally used is supported by work on individual spin-coated PS:PnBA films (Stenert *et al.*, 2004). In the system PS:PnBA the majority component forms a matrix which embeds the minority component as disperse objects irrespective of the actual blend ratio.

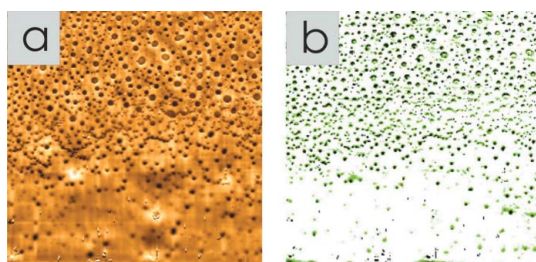


Figure 6
(a) Topography probed with the AFM (scan area 60 $\mu\text{m} \times 60 \mu\text{m}$) after subtracting the macroscopic height profile to emphasize the lateral structures. (b) Corresponding phase image covering a z range from -2.7 V (dark) to -0.7 V (light) showing the mechanical response. Flow is directed along the vertical axis.

Flow-induced structures, as described in this section, are not accessible in standard GISAXS experiments. GISAXS typically makes use of X-ray beams with a size comparable to the region shown in the optical micrograph (see Fig. 4). Thus within the beam diameter the sample is neither homogeneous with respect to the type of structure nor does it have one mean surface, which is necessary for the definition of the reflection geometry inherent to GISAXS. With sub-microbeam GISAXS both problems are overcome. Applying the conditions described in §2, the beam reduces to a stripe, which is indicated by the solid line in Fig. 4. The long side of the footprint is oriented perpendicular to the flow direction, allowing a set of scans at different y positions along it.

It is obvious that an experiment with a beam diameter of 0.9 μm is not suited to probing micrometre-size structures. Thus with sub-microbeam GISAXS, small structures which are located inside the film or at the film surface will be under investigation.

In a typical sub-microbeam GISAXS experiment the region of interest is pre-selected by optical microscopy. Calibration of the optics with respect to the X-ray beam allows a controlled local scattering experiment. By scanning the sample with respect to the X-ray beam (movement along the y direction) and performing consecutive GISAXS experiments, the region of interest is mapped. In the experiment presented here a range of 50 μm centered on the SPM data shown in Fig. 6 has been scanned. Steps of $\Delta y = 1 \mu\text{m}$ were selected. Instead of displaying 50 GISAXS patterns or 50 horizontal cuts, Fig. 7 shows an alternative presentation. The characteristic features of 50 GISAXS patterns are extracted by composing respective horizontal cuts at the critical angle of PS for different y positions into one (yq_y) map. The central region around $q_y = 0$ is dominated by the relaxed resolution of the sub-microbeam GISAXS setup. The observed high intensity is characteristic for large lateral lengths, as displayed in the SPM and optical data. The color bar in Fig. 7 is adapted to focus on small length scales comparable to the size of the polymer molecules. At large q_y values widespread peaks are visible on the left and right. The corresponding lateral structure is on

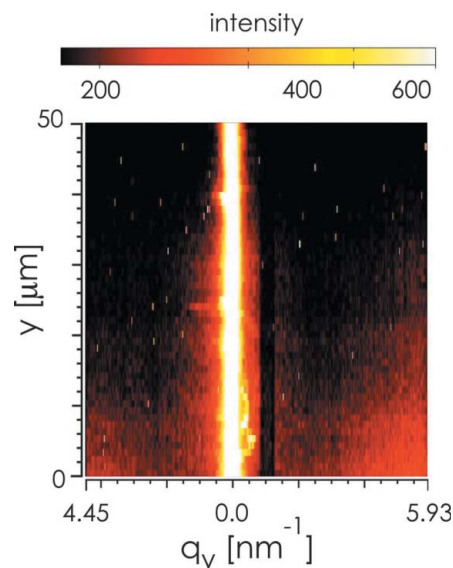


Figure 7
With sub-microbeam GISAXS a region of 50 μm is scanned in steps of $\Delta y = 1 \mu\text{m}$. Full ($y\psi$) mapping: all horizontal cuts are plotted from the 2D sub-microbeam GISAXS data as a function of the out-of-plane angle ψ at the scanning position y . The black vertical stripe at $q_y \approx 1 \text{ nm}^{-1}$ originates from the shadow of the beamstop holder needed to protect the sensitive detector against the intense specular peak in GISAXS.

the nanometre scale. Comparing Figs. 6 and 7, this nanometre-size structure only exists in the part of the polymer bulge (bottom part of Fig. 6). Regions with larger PnBA content do not show any substructure. From SPM we have no indication that the structure is located at the surface. Consequently, the structure is located inside the polymer bulge. It is very likely that this structure results from the different mechanical properties of the majority component. Cavities introduced by the competition of flow and drying relax in the case of remaining mobility of the matrix and no nanostructure is observed in PnBA-rich regions. With increasing amounts of PS this relaxation is suppressed and nanometre-size cavities remain in the PS-rich regions. Glassy materials, such as PS, typically show a tendency to form crazes under mechanical load. The size of such crazes is of similar scale, depending on the stress induced (Lorenz-Haas *et al.*, 2003).

5. Summary and outlook

Simply blending two immiscible polymers in a solvent solution, such as PS and PnBA in toluene, and solution casting this blend solution onto an Si support, easily results in film structures. These are difficult to probe with standard GISAXS. Real-space investigations with optical and scanning-probe techniques give quick access to the surface structures, whereas internal structures remain unknown. Owing to recent experimental developments, accessible at different synchrotron beamlines, advanced GISAXS setups have become possible. With high resolution in reciprocal and real space at these highly optimized beamlines, the difficulties of standard GISAXS are overcome.

With GIUSAXS a strong overlap with the optical regime is achieved. Theoretically, structures up to 21 μm are resolvable, which is a major breakthrough for all large-scale structured systems, such as polymer-blend films. Moreover, biological systems, colloids, or porous foams easily exhibit structures on a comparable scale. GIUSAXS provides a tool for probing internal structures in such systems as well. With sub-microbeam GISAXS a local scattering experiment is possible. Averaging is only performed along the elongated footprint of the micrometre-size beam and over the probed sample depth. Thus local spots on a sample or extremely small samples can be accessed, which is vital for the investigation of more complex systems, such as flow-induced structures. As demonstrated here, gradient-type samples combine many of the ideas of high-throughput investigations (Roth *et al.*, 2003, 2006) and dramatically shorten the time needed to achieve a desired surface morphology.

In summary, whereas within this article we only studied a simple blend film system, with advanced GISAXS a dramatically larger

number of different sample systems becomes analyzable. However, at present these experiments will remain restricted to highly specialized synchrotron beamlines and will not be easily transferred to a standard GISAXS measuring station.

We thank M. Stenert and F. Bandermann for supplying the PnBA, C. David for providing the Fresnel-zone plates used at ID13, and the BMBF (Förderkennzeichen 03CO333) and the DFG SPP 1164 'Nano- and Microfluidics' (Mu1487/2) for financial support.

References

- Gibaud, A., Grosso, D., Smarsly, B., Baptiste, A., Bardeau, J. F., Babonneau, J., Doshi, D. A., Chen, Z., Brinker, C. J. & Sanchez, C. (2003). *J. Phys. Chem. B*, **107**, 6114–6118.
- Gutmann, J. S., Müller-Buschbaum, P. & Stamm, M. (1999). *Faraday Discuss.* **112**, 285–297.
- Hashimoto, T. (1993). *Material Science and Technology*, edited by R. W. Cahn, Vol. 12, pp. 251–300. Weinheim: VCH.
- Levine, J. R., Cohen, J. B., Chung, Y. W. & Georgopoulos, P. (1989). *J. Appl. Cryst.* **22**, 528–532.
- Lorenz-Haas, C., Müller-Buschbaum, P., Wunnicke, O., Cassagnol, C., Burghammer, M., Riekel, C. & Stamm, M. (2003). *Langmuir*, **19**, 3056–3061.
- Müller-Buschbaum, P. (2003a). *Anal. Bioanal. Chem.* **376**, 3–10.
- Müller-Buschbaum, P. (2003b). *Euro. Phys. J. E*, **12**, 443–448.
- Müller-Buschbaum, P. (2006). *Prog. Colloid. Polym. Sci.* **132**, 23–32.
- Müller-Buschbaum, P., Bauer, E., Pfister, S., Roth, S. V., Burghammer, M., Riekel, C., David, C. & Thiele, U. (2006). *Europhys. Lett.* **73**, 35–41.
- Müller-Buschbaum, P., Roth, S. V., Burghammer, M., Diethert, A., Panagiotou, P. & Riekel, C. (2003). *Europhys. Lett.* **61**, 639–645.
- Müller-Buschbaum, P., Vanhoorne, P., Scheumann, V. & Stamm, M. (1997). *Europhys. Lett.* **61**, 655–660.
- Papadakis, C. M., Busch, P., Posselt, D. & Smilgies, D. M. (2004). *Adv. Solid State Phys.* **44**, 327–338.
- Renaud, G., Revenant-Brizard, C., Lazzari, R., Barbier, A., Noblet, M., Ulrich, O., Borenstzeim, Y., Jupille, J., Henry, C. R., Deville, J. P., Scheurer, F. & Fruchart, O. (2003). *Science*, **300**, 1416–1419.
- Riekel, C. (2000). *Rep. Prog. Phys.* **63**, 233–262.
- Roth, S. V., Burghammer, M., Riekel, C., Müller-Buschbaum, P., Diethert, A., Panagiotou, P. & Walter, H. (2003). *Appl. Phys. Lett.* **82**, 1935–1937.
- Roth, S. V., Walter, H., Burghammer, M., Riekel, C., Lengeler, B., Schroer, C., Kuhlmann, M., Walther, T., Sehrbrock, A., Domnick, R. & Müller-Buschbaum, P. (2006). *Appl. Phys. Lett.* **88**, 021910–021912.
- Ryan, A. J. (2002). *Nature Mater.* **1**, 8–10.
- Salditt, T., Metzger, T. H., Peisl, J., Reinker, B., Moske, M. & Samwer, K. (1995). *Europhys. Lett.* **32**, 331–336.
- Stenert, M., Doring, A. & Bandermann, F. (2004). *e-Polymers*, **15**, 1–16.
- Tanaka, H. (2000). *J. Phys. Condens. Matter*, **12**, R207–R264.
- Walheim, S., Schäffer, E., Mlynek, J. & Steiner, U. (1999). *Science*, **283**, 520–522.
- Wang, H. & Composto, R. J. (2003). *Inter. Sci.* **11**, 237–248.
- Yang, K. & Han, C. D. (1996). *Polymer*, **37**, 5795–5805.